Atmospheric
Chemistry
and Physics

Supplement of

Mapping the dependence of black carbon radiative forcing on emission region and season

Petri Räisänen et al.

*Correspondence to:* Petri Räisänen (petri.raisanen@fmi.fi)

This Supplementary material contains ten figures. These figures are related to the following sections of the main paper:
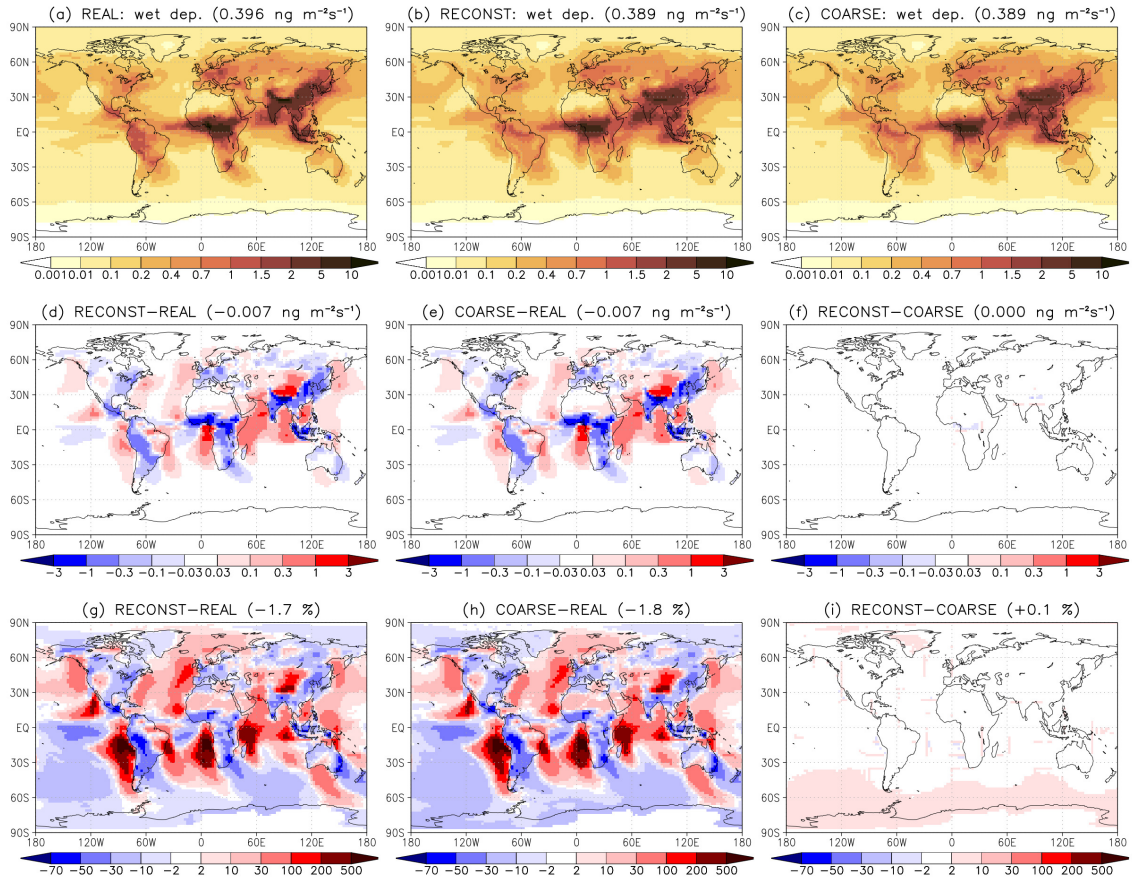
- Figures S1–S5: Sect. 4.2 (Additivity and linearity of BC radiative forcings)

- Figure S6: Sect 5.1 (Example: Radiative forcing for emissions in Fennoscandia)

- Figure S7: Sect. 5.2 (Impact of emisision location)
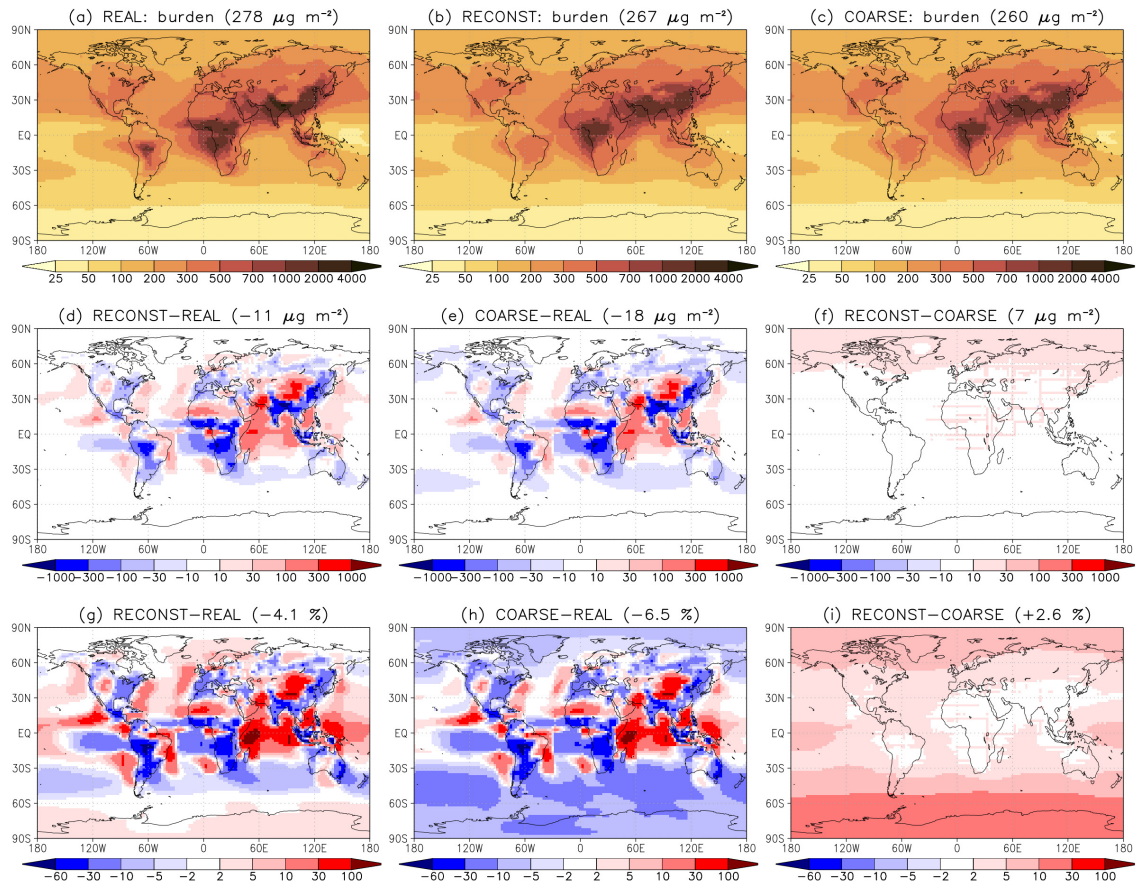
5
- Figures S8–S10: Sect. 5.3 (Impact of emission season)
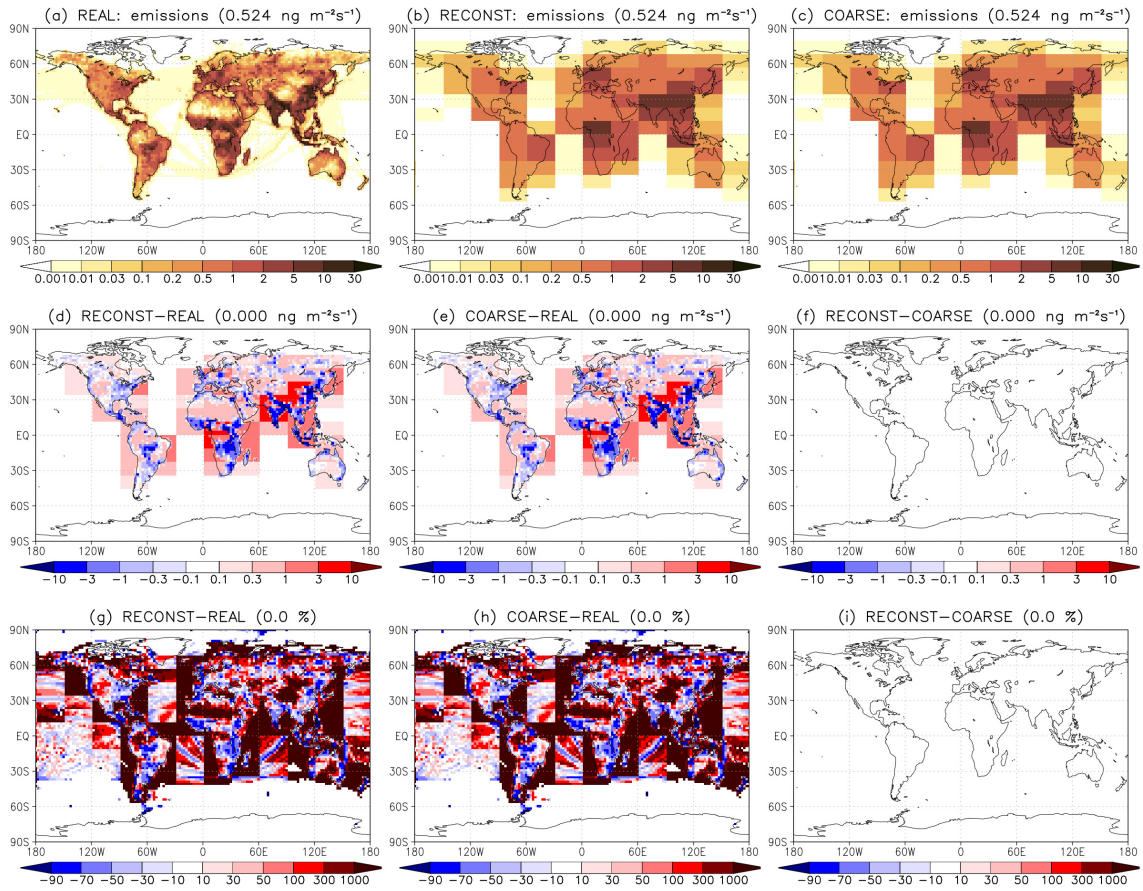
Figure S1. BC emissions (in units of $\mathrm{ng\,m^{-2}\,s^{-1}} = 10^{-12}\,\mathrm{kg\,m^{-2}\,s^{-1}}$) in the experiments (a) REAL and (c) COARSE. Between them, (b) shows the emissions reconstructed using Eq. (4) in the main paper, which are identical for the two experiments. (d) Reconstruction errors $(\mathrm{ng\,m^{-2}\,s^{-1}})$ for REAL. To aid comparison with other similar figures (Figs. 1 and 2 in the main paper and Figs. S2–S5 in this Supplement) these errors are further decomposed into two parts, where (e) the difference COARSE−REAL represents the emission error arising from the inability of the reconstruction to represent accurately the emissions in REAL, and (f) the difference RECONST−COARSE (i.e., the reconstruction error for COARSE) is the additivity error that arises from nonadditivity and nonlinearity when combining the effect of BC emissions for different regions and seasons. In the case of reconstructed emissions, this decomposition is, however, trivial: the reconstruction error for REAL equals the emission error and the additivity error is zero everywhere. (g)–(i) Relative errors corresponding to (d)–(f) (in %). Global-mean values are indicated in the panel titles.
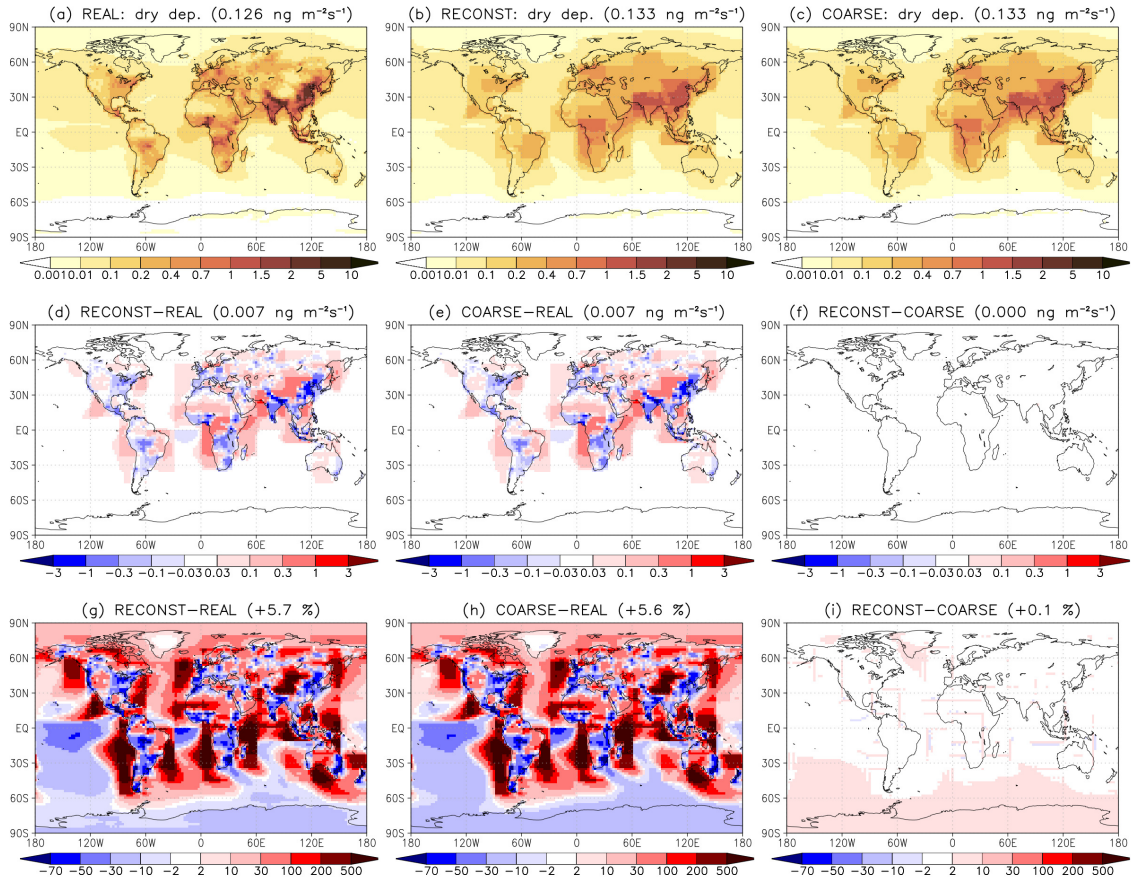
Figure S2. BC dry deposition rate (in units of $\mathrm{ng\,m^{-2}\,s^{-1} = 10^{-12}\,kg\,m^{-2}\,s^{-1}}$) in the experiments (a) REAL and (c) COARSE. Between them, (b) shows the dry deposition rate reconstructed using Eq. (4) in the main paper, which is identical for the two experiments. (d) Reconstruction errors $(\mathrm{ng\,m^{-2}\,s^{-1}})$ for REAL. These errors are further decomposed into two parts, where (e) the difference COARSE−REAL represents the emission error arising from the inability of the reconstruction to represent accurately the emissions in REAL, and (f) the difference RECONST−COARSE (i.e., the reconstruction error for COARSE) is the additivity error that arises from nonadditivity and nonlinearity when combining the effect of BC emissions from different regions and seasons. (g)–(i) Relative errors corresponding to (d)–(f) (in %). Global-mean values are indicated in the panel titles.

3

Figure S3. BC wet deposition rate (in units of $\mathrm{ng\,m^{-2}\,s^{-1}} = 10^{-12}\,\mathrm{kg\,m^{-2}\,s^{-1}}$) in the experiments (a) REAL and (c) COARSE. Between them, (b) shows the wet deposition rate reconstructed using Eq. (4) in the main paper, which is identical for the two experiments. (d) Reconstruction errors $(\mathrm{ng\,m^{-2}\,s^{-1}})$ for REAL. These errors are further decomposed into two parts, where (e) the difference COARSE−REAL represents the emission error arising from the inability of the reconstruction to represent accurately the emissions in REAL, and (f) the difference RECONST−COARSE (i.e., the reconstruction error for COARSE) is the additivity error that arises from nonadditivity and nonlinearity when combining the effect of BC emissions from different regions and seasons. (g)–(i) Relative errors corresponding to (d)–(f) (in %). Global-mean values are indicated in the panel titles.

4

Figure S4. BC burden (in units of $\mu g\,m^{-2} = 10^{-9}\,kg\,m^{-2}$) in the experiments (a) REAL and (c) COARSE. Between them, (b) shows the BC burden reconstructed using Eq. (4) in the main paper, which is identical for the two experiments. (d) Reconstruction errors ($\mu g\,m^{-2}$) for REAL. These errors are further decomposed into two parts, where (e) the difference COARSE−REAL represents the emission error arising from the inability of the reconstruction to represent accurately the emissions in REAL, and (f) the difference RECONST−COARSE (i.e., the reconstruction error for COARSE) is the additivity error that arises from nonadditivity and nonlinearity when combining the effect of BC emissions from different regions and seasons. (g)–(i) Relative errors corresponding to (d)–(f) (in %). Global-mean values are indicated in the panel titles.
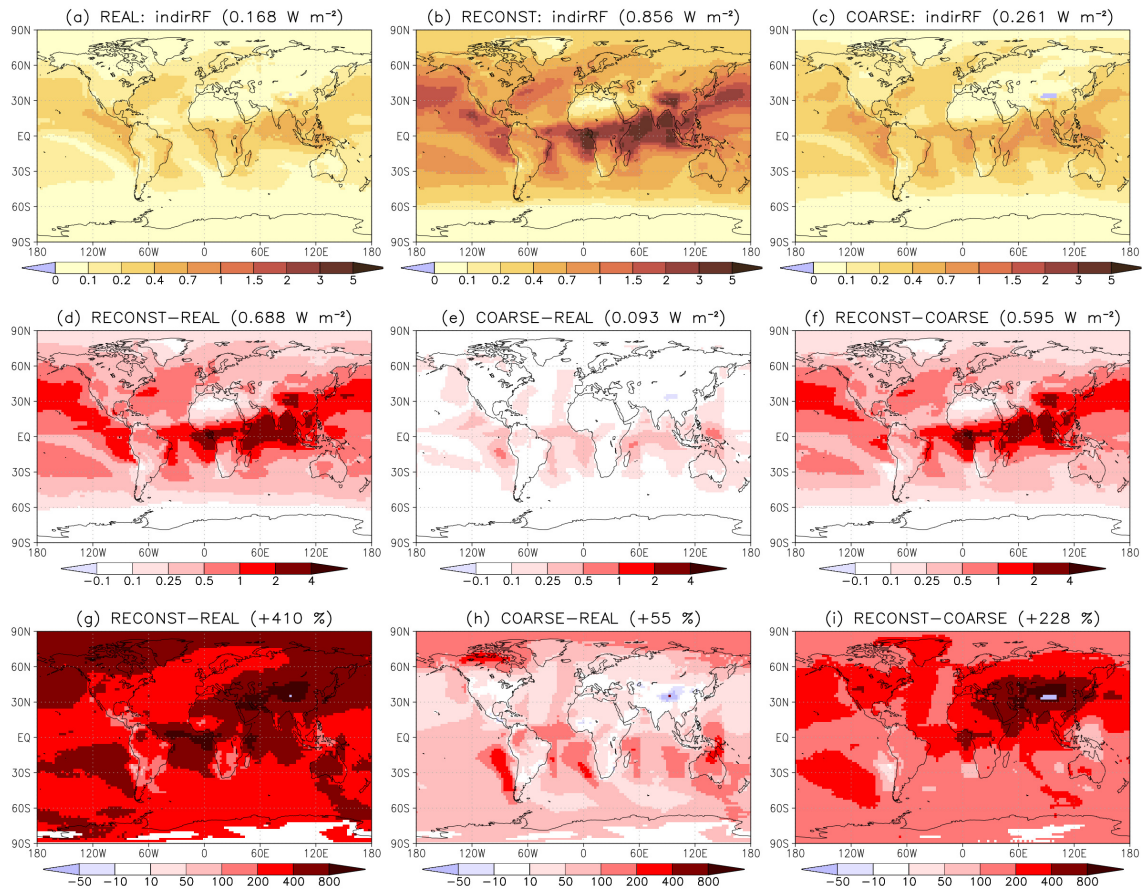
Figure S5. BC indirect radiative forcing at TOA ($W\,m^{-2}$) in the experiments (a) REAL and (c) COARSE. Between them, (b) shows indirRF reconstructed using Eq. (4) in the main paper, which is identical for the two experiments. (d) Reconstruction errors ($W\,m^{-2}$) for REAL. These errors are further decomposed into two parts, where (e) the difference COARSE−REAL represents the emission error arising from the inability of the reconstruction to represent accurately the emissions in REAL, and (f) the difference RECONST−COARSE (i.e., the reconstruction error for COARSE) is the additivity error that arises from nonadditivity and nonlinearity when combining the effect of BC emissions from different regions and seasons. (g)–(i) Relative errors corresponding to (d)–(f) (in %). Global-mean values are indicated in the panel titles.
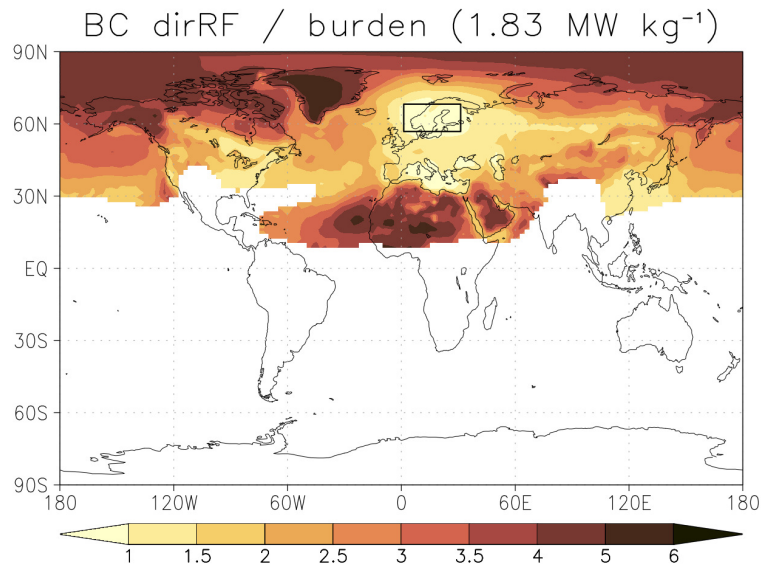
Figure S6. Ratio of BC direct radiative forcing to BC burden (MW kg^{-1}) for the experiment in which a constant BC emission rate of 10^{-12} kg m^{-2} s^{-1} was applied in the lat-lon box 56.84–68.21°N, 1.25–31.25°E (shown with a rectancle). Regions with very small BC burden (below 10^{-10} kg m^{-2}) are screened out. The global mean value is indicated in the figure title. High values are seen for BC over high-albedo surfaces such as Greenland, the northernmost parts of North America, central Arctic Ocean, and over the Sahara and Arabian deserts. Also, the values are enhanced where much of BC resides above clouds, e.g. in the norhernmost parts of the Pacific and Atlantic oceans and west of Sahara. In contrast, low values occur where BC is preferentially located below clouds; most notably in the emission region where much of the BC resides close to the surface.
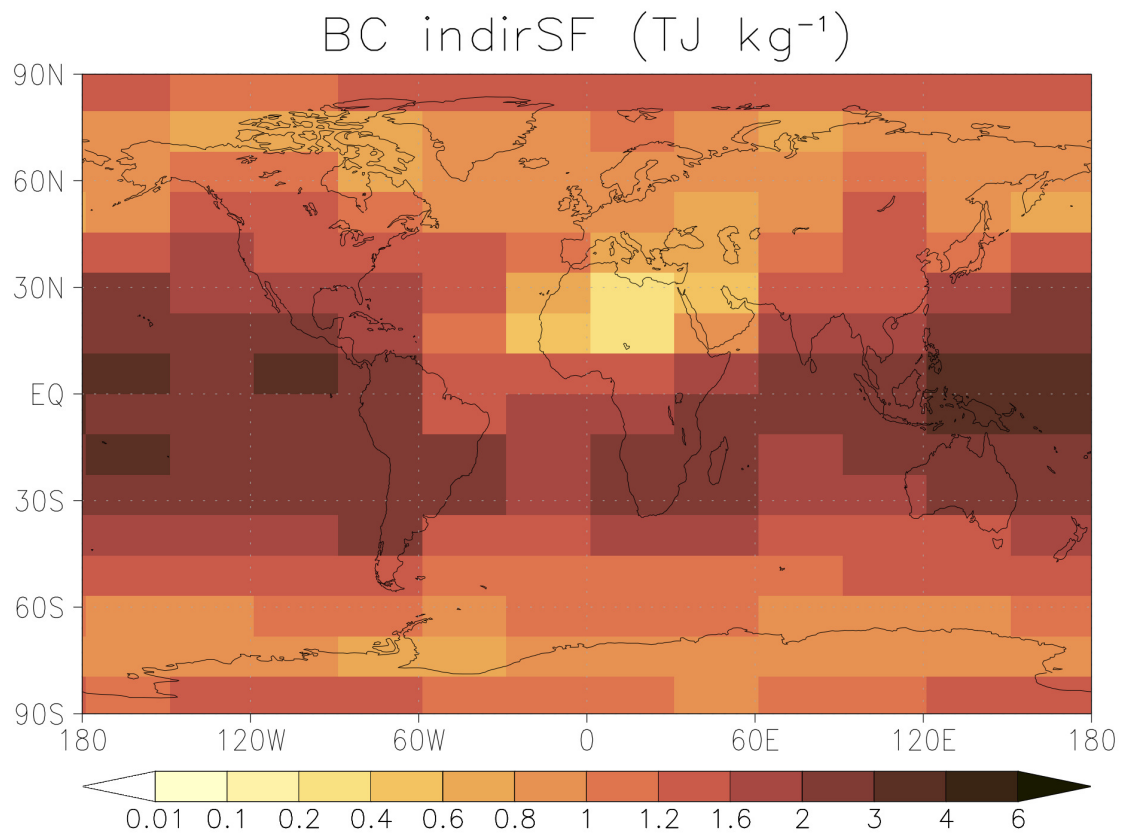
Figure S7. Global-mean values of BC indirect specific forcing $(TJ\,kg^{-1})$ for the experiments in which uniform BC emissions over the year were assumed, separately for emissions in each of the 192 lat-lon boxes.
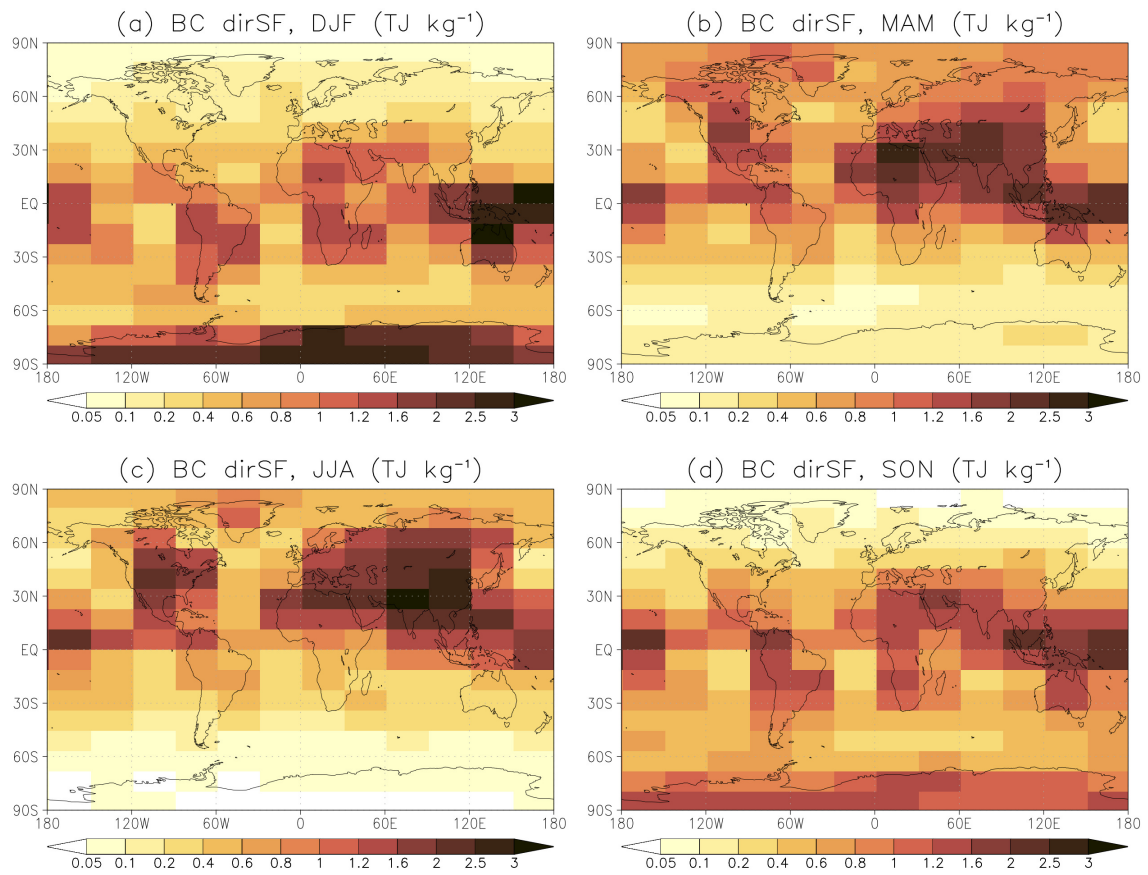
Figure S8. Global-mean values of BC direct specific forcing (in units of $TJ\,kg^{-1}$) separately for emissions in 192 lat-lon boxes, for emissions in (a) DJF, (b) MAM, (c) JJA and (d) SON.
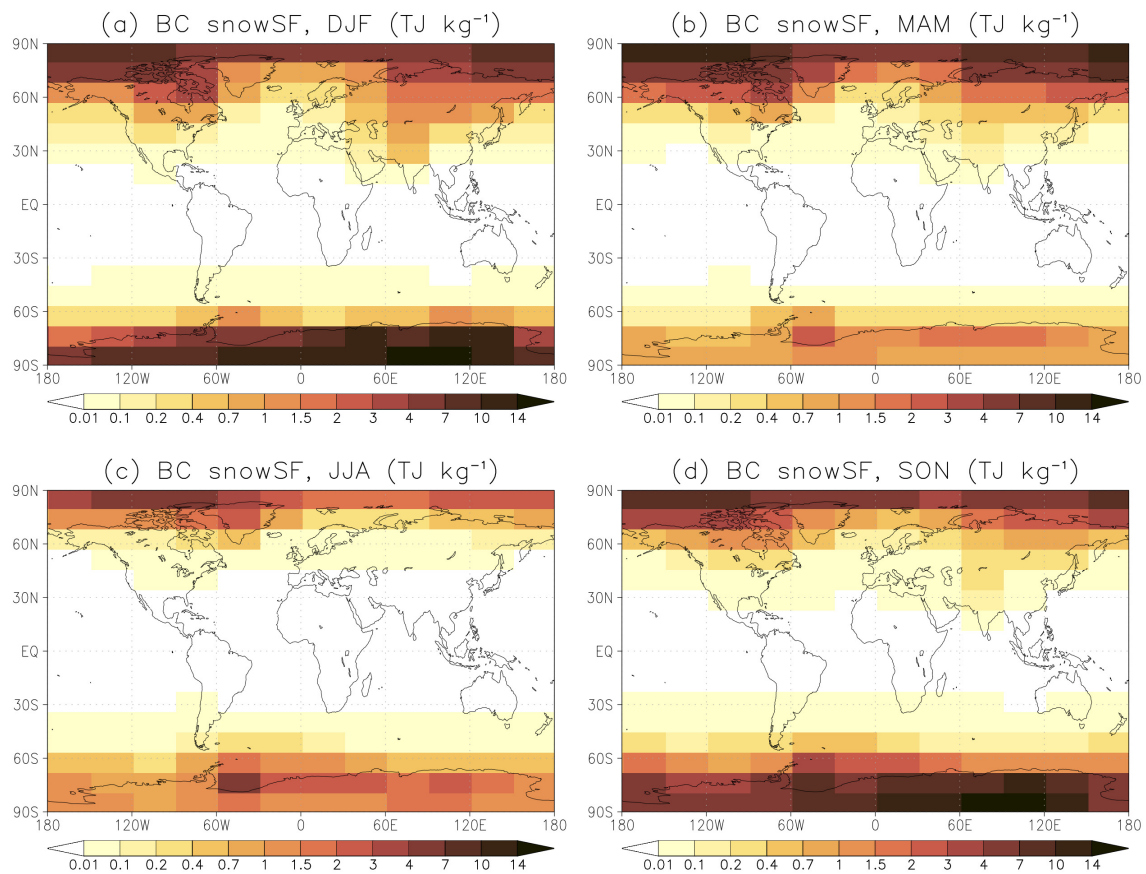
Figure S9. Global-mean values of specific forcing due to BC in snow (in units of $\mathrm{TJ\,kg^{-1}}$) separately for emissions in 192 lat-lon boxes, for emissions in (a) DJF, (b) MAM, (c) JJA and (d) SON.
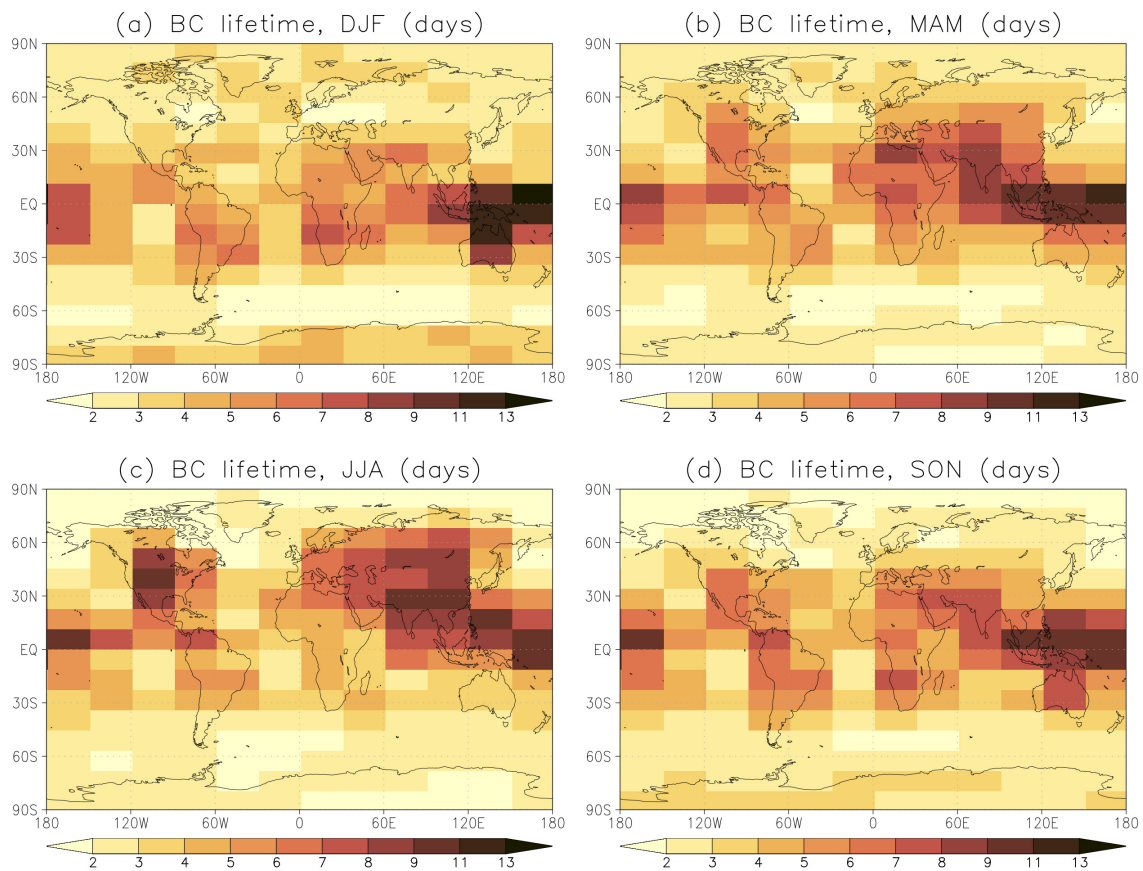
Figure S10. BC lifetime (days) separately for emissions in 192 lat-lon boxes, for emissions in (a) DJF, (b) MAM, (c) JJA and (d) SON.